Repair of Internal and External Circular Failures Using Winding Technology

B. Pere[1], J. Égert[1] and T. Szabó[2]

[1]Széchenyi István University, Department of Applied Mechanics
[2]University of Miskolc, Robert Bosch Department of Mechatronics

The first part of the paper deals with the FEM computation of deformations, stresses and strain in the surrounding area of internal and external circular artificial failures with a set of given geometrical dimensions in steel pipelines. For the investigation of this problem three groups of mechanical models are applied: multilayered elastic shell, 3D elastic solid and 3D elastic-plastic solid FEM models. The aim of this analysis is to clarify the case in which the pipeline fails. When a pipe fails and needs repair or reinforcement, this is called critical case.

In the second part of the paper the repaired pipes are investigated. For repairing of the internal and external failures, internal or external multilayered textile composite reinforcements are applied by winding technology. The task is to determine the width of the reinforcement and the number of layers needed for repair.

The different mechanical models (multilayered elastic shell, 3D elastic solid and 3D elasto-plastic solid) are compared on the basis of numerical results. The critical cases are determined and the questions of repair are answered also numerically.

Keywords: Steel pipeline, artificial circular damage, textile composite reinforcement, FEM analysis, elastic shell and 3D elastic-plastic modelling

1. Introduction

Oil and gas pipelines often have internal and external circular failures. The internal failures usually originate from welding on location, and the external failures result from any other violent external effect, for instance due to agricultural equipment working above the pipeline.

The first task is to predict the risk caused by these circular failures. In the first step one needs to clarify the deformations, stresses and strains around the damaged part of the pipe. On the basis of such analysis one can find critical cases in which repairs are needed.

The second task is to fix or to repair the damaged pipe. In this paper an internal or external multilayered textile composite reinforcement are applied at the location of the failures. The multilayered textile composite reinforcement is made by winding technology. During the design of this composite reinforcement the width and the number of layers of the winding should be determined. The failures are considered to be fixed when stresses are below the critical values both in the steel pipe and in the composite reinforcement.

The numerical aspects of both tasks are discussed in this paper. In the first step two kinds of circular damaged pipe-parts using the finite element method and the I-DEAS program code are investigated. The failures may have a high number of varieties therefore two typical artificial failure geometries are chosen. On the basis of the numerical analysis the critical cases have been determined in which repairs are needed. In the second step an internal and/or external composite reinforcement with different widths and numbers of layers are applied for the critical cases. When analyzing critical cases the proper width and number of layers of reinforcement can be found.

2. Geometry of typical artificial failures and reinforcements

Fig. 1. shows the global geometry i.e. the location of the investigated internal and external circular failures.
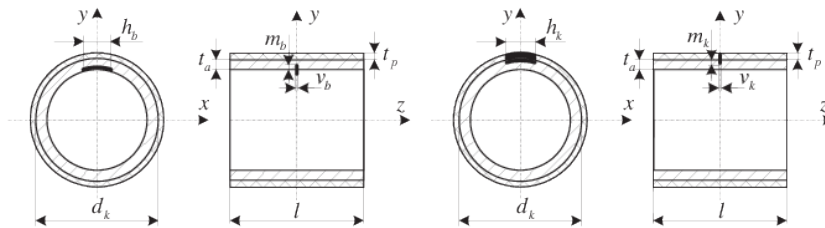
Figure 1. Global geometry of the internal and external circular failures

The steel pipe's external diameter is $d_k = 323,9$ mm, its wall thickness is $t_a = 7,1$ mm and the length of the investigated pipe part is $l = 2000$ mm. The steel pipe is coated with a $t_p = 3,12$ mm thick polyethylene insulation layer against corrosion. The longitudinal dimension of the circular failures are $h_b = h_k = 150$ mm for both internal and external cases, the width is $v_b = 1,5$ mm for the internal case and $v_k = 2$ mm for the external case. There are three depth versions $m_b = m_k = 2; 4; 6$ mm investigated.

Fig. 2. shows the local geometry of analyzed internal and external circular failures. The geometry of the artificial failures (Fig. 2.) can be easily reproduced later for the planned experiments.
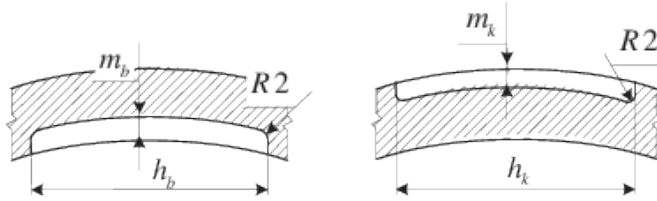
Figure 2. Local geometry of the internal and external circular failures

Internal and external circular failures of pipes can be reinforced theoretically from the outside or the inside as well. Fig. 3. shows the reinforcement possibilities for an internal failure. At the location of the failure the anti-corrosion layer is removed and the reinforcement is winded directly to the steel surface.

The layer thickness of reinforcement in each case is the same $t_k = t_b = 0,3$ mm, and three different widths of the winding bands are investigated $s_k = s_b = 50; 100; 200$ mm.
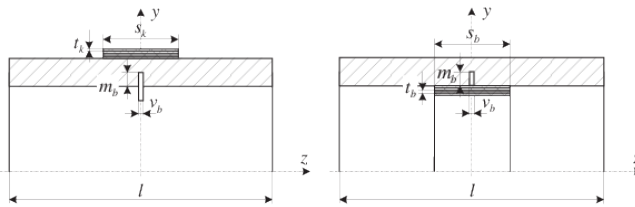
Figure 3. Reinforcement versions for the internal circular damage

3. Mechanical modelling of the materials and working conditions

The pipe is made of steel, the protecting layer against corrosion is polyethylene and the material of the reinforcement is carbon fiber textile reinforced plastics (CFRP). From the mechanical point of view the steel and the polyethylene are modelled as linear elastic materials given by two material constants, the yield strength and ultimate strength. These material parameters in Table 1 are measured by the Department of Mechanical Technology of Miskolc University [7].

In Table 1 E is the modulus of elasticity, ν is the Poisson's ratio, $\mathbf{R_{t0,5}}$ is the yield limit and $\mathbf{R_m}$ is the breaking strength of material.

In linear elastic, isotropic, plane stress problems the following Hooke's law provides the

Material	E [MPa]	ν [–]	$R_{t0,5}$ [MPa]	R_m[MPa]
Steel	205 000	0,3	499	603
Polyethylene	527	0,31	–	12,8

Table 1. Material constants and ultimate stress values

constitutive equations:

$$\varepsilon_1 \varepsilon_2 \gamma_{12} = 1E - \nu E 0 - \nu E 1 E 000 2(1+\nu)E \sigma_1 \sigma_2 \tau_{12}, \tag{1}$$

1 and 2 are directions perpendicular to each other in the tangent plane of the middle surface of the pipe. $\varepsilon_1, \varepsilon_2$ and σ_1, σ_2 are strains and normal stresses in direction 1, 2 respectively. γ_{12} and τ_{12} are the in-plane shear strain and the shear stress.

The elasto-plastic computations are carried out by using the stress-strain diagram in Fig. 4. given by the Department of Mechanical Technology of Miskolc University [7].
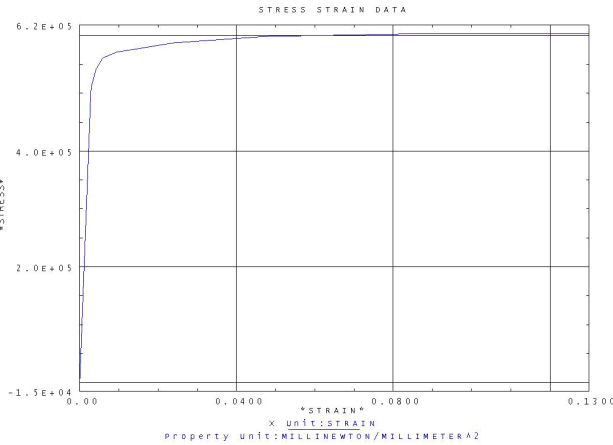
Figure 4. Stress-strain diagram of the steel pipe

For isotropic materials the well known von Mises failure criterium is applied:

$$12 \left(1 R_{t0,5}\right)^2 \left[(\sigma_I - \sigma_{II})^2 + (\sigma_{II} - \sigma_{III})^2 + (\sigma_I - \sigma_{III})^2 \right] \leq 1, \quad \text{or} \tag{2}$$

$$\sigma_{red\,max} \leq R_{t0,5}, \tag{3}$$

where $\sigma_I, \sigma_{II}, \sigma_{III}$ are the principal stresses.

According to references [1], [2], the carbon fiber textile reinforced composite can be modelled from the macroscopic point of view by an orthotropic constitutive law:

$$\varepsilon_1 \varepsilon_2 \gamma_{12} = 1E_1 - \nu_{12}E_20 - \nu_{21}E_11E_20001G_{12}\sigma_1\sigma_2\tau_{12}, \tag{4}$$

In the above equations the indices 1, 2 stand for the principal material direction of CFRP. In the constitutive law E_1, E_2 are orthotropic moduli of elasticity, ν_{12}, ν_{21} are Poisson's ratios and G_{12} is the independent in-plane shear modulus. The Poisson's ratios are not independent from each other and due to energy reasons [2] the following relation exists :

$$\frac{\nu_{12}}{E_2} = \frac{\nu_{21}}{E_1}. \tag{5}$$

Macroscopic modelling means that equations are not appropriate to determine stresses and strains in the carbon fibers or in the matrix material, but do well for a larger area with a lot of fibers. Therefore, the above stresses and strains are the average features of an area with a lot of fibers.

For the orthotropic material the Tsai-Wu's failure criterium is applied:

$$\sigma_1^2 \sigma_{H1}\sigma_{D1} + \sigma_2^2 \sigma_{H2}\sigma_{D2} - \sigma_1\sigma_2\sqrt{\sigma_{H1}\sigma_{D1}\sigma_{H2}\sigma_{D2}} + \tau_{12}^2\tau_{S12}^2 +$$

$$+ \left(1\sigma_{H1} - 1\sigma_{D1}\right)\sigma_1 + \left(1\sigma_{H2} - 1\sigma_{D2}\right)\sigma_2 \leq 1, \tag{6}$$

or

$$K_{tw} \leq 1, \tag{7}$$

where σ_{H1}, σ_{H2} are tensile, σ_{D1}, σ_{D2} are compressive and τ_{S12} is shear strengths.

Table 2 contains the measured material constants and ultimate stress values of the applied CFRP measured by the Department of Polymer Engineering of the Budapest University of Technology [8].

The deformations, stresses and strains in the damaged pipe and in the reinforced pipe are determined for two loading cases, i.e. for a normal working condition and for a loading condition, that can be verified by an experiment.

Thickness [mm]	E_1 [MPa]	E_2 [MPa]	ν_{12} [–]	G_{12} [MPa]
0,3	47 600	45 000	0,036	2 000

σ_{H1} [MPa]	σ_{H2} [MPa]	σ_{D1} [MPa]	σ_{D2} [MPa]	σ_{S12} [MPa]
436	430	310	340	76

Table 2. Material constants and ultimate stress values of CFRP layers
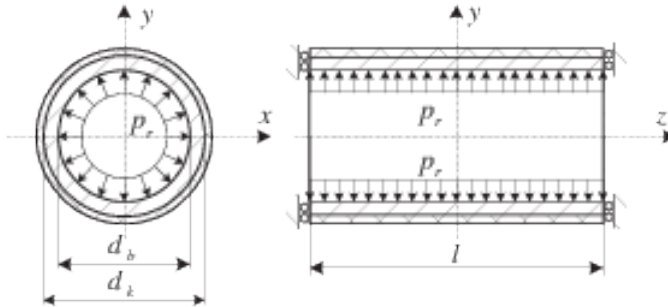
Figure 5. Mechanical model for normal working condition

In normal working conditions the pipeline is embedded in the earth which does not allow the longitudinal displacements of the investigated pipe parts. This is the reason why the mechanical model is clamped at both ends of the pipe part in the normal working loading case. There is a $p_r = 63$ bar internal pressure in both loading cases in the pipe.
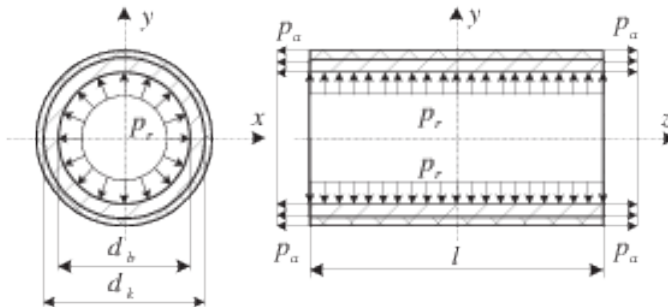
Figure 6. Mechanical model for experimental checking

In the experiments the investigated pipe part is closed at both ends. The internal pressure provides an $p_a = d_b^2 p_r \left(d_k^2 - d_b^2 \right)$ additional axial loading because of the closed ends. So the experimental loading case consists of the internal pressure and the axial loading.

4. Finite element approaches and meshes

For computation of deformations, stresses and strains around the circular failures the following three models are applied: multilayered elastic shell, 3D elastic solid and 3D elasto-plastic solid elements. However computations of repaired pipes are carried out only by multilayered elastic shell elements.

By using layered shell elements it is possible to model failures by proper choice of layer thicknesses. Fig. 7. shows two cases for the proper thickness choice. The left one is at a common location of the pipe and the right one is at an internal failure with 4 mm depth. In both cases in Fig. 7. the upper layer represents the insulation and two internal layers for modelling the internal failure are shown in the right picture. Naturally, for the failure area zero values should be given for material constants.

Thickness	Angle	Ply		Material		Thickness	Angle	Ply		Material
3.12	+0	5		INSULATION		3.12	+0	5		INSULATION
1.1	+0	4		STEEL		1.1	+0	4		STEEL
2	+0	3		STEEL		2	+0	3		STEEL
2	+0	2		STEEL		2	+0	2		FAILURE
2	+0	1		STEEL		2	+0	1		FAILURE

Figure 7. Modelling of failure thickness by multilayered shell elements

Fig. 8. shows two cases for the proper thickness choice of layers at reinforcement. The left and right pictures represent the thicknesses of layers in undamaged and damaged locations, respectively.

Using multilayered shell elements it is only possible to apply a sharp corner approach for failures, so the R2 mm rounding in Fig. 2. is not taken into consideration at shell modelling.

The 3D modelling allows a very accurate approach of real geometry of artificial internal and external failures, even an R2 mm rounding.
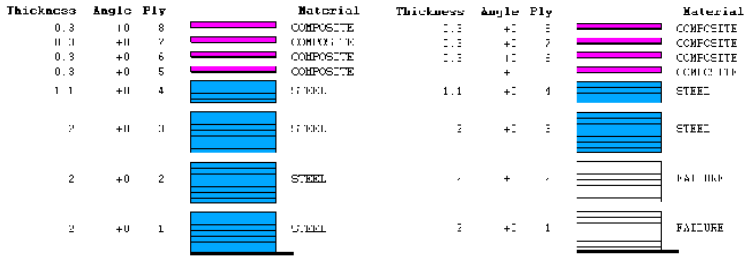
Figure 8. Modelling of reinforcement and failure thickness by shell elements

	Shell model	3D solid model
Number of elements	5 000	17 500
Number of nodes	15 000	36 000

Table 3. Characteristic data for FEM meshes

Table 3 includes the parameters of the applied meshes. The nodes of shell elements have six degrees of freedom and the nodes of 3D solid elements three, so one has to solve in both tasks a linear algebraic equation system with about 90-108 thousand unknowns. The computations for both shell and 3D solid modelling are carried out also with much denser mesh in order to prove that the applied mesh provides accurate results.

When creating finite element meshes the double symmetry is taken into account. Naturally, the mesh is much denser around the failures than at the other areas of the model in the interest of accuracy of computations.

Fig. 9. shows an example for a shell model and a mesh part for a 3D solid model. The $l_m = l/2 = 1000$ mm length of mesh is chosen so that the influence of the boundary conditions at the end of the pipe part and the influence of the circular failure do not disturb each other.

On the basis of computational experience it is enough to apply shorter models with $l_r = l_m/2 = 500$ mm length for the computation of reinforced pipe parts. In these meshes

one has to take into consideration the width of the reinforcing composite band at meshing (Fig. 10.).

5. Numerical results of analysis

5.1. Influence of insulation layer

The analysis of the influence of the external polyethylene insulation is carried out only for internal circular failure. Numerical results prove that the insulation layer has no importance from the mechanical point of view, since the stiffness of the insulation layer is negligible compared to the steel's stiffness. Therefore the insulation layer is neglected in the investigations.
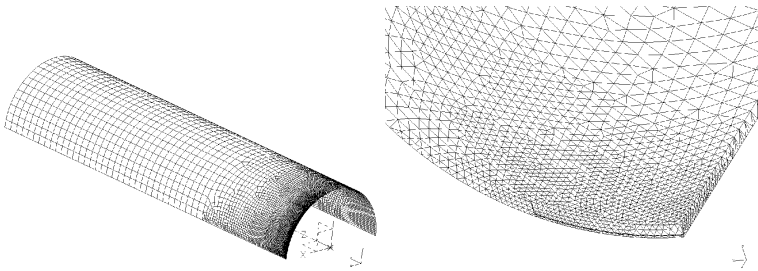
Figure 9. Shell mesh and 3D solid mesh part for circular failure
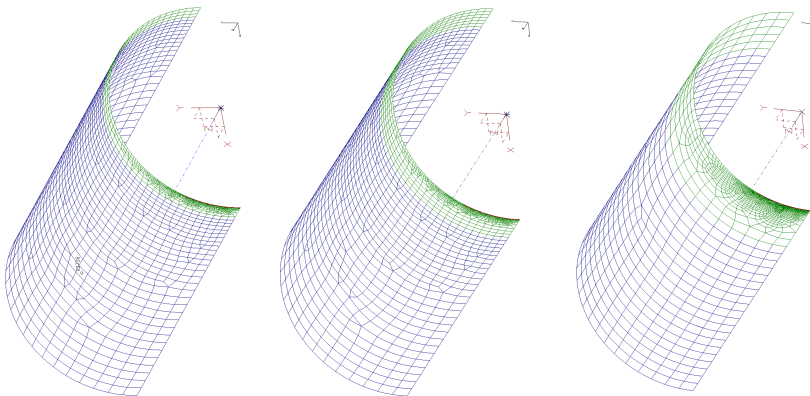
Figure 10. Shell meshes for different reinforcements

5.2. Results of damaged steel pipes

The characteristics of deformations and stress/strain distributions is similar for both loading cases. However the critical values of deformations, stresses and strains are a little higher for the experimental checking than for the normal loading conditions. This is the consequence of the additional axial loading originated from the internal pressure. This axial loading seems to be a little higher than the axial loading originated from the clamped ends of the pipe model at normal working conditions. Therefore, only the results of this hazardous experimental loading case are presented in this paper.

Numerical results show that the deformation of pipes with internal failure depends significantly on the depth of failure. Fig. 11-13. demonstrates these differences on the radial displacement distribution of the middle surface. It is very interesting that the maximum deformation occurs not directly at the failure but beside that. Fig. 14-16 shows
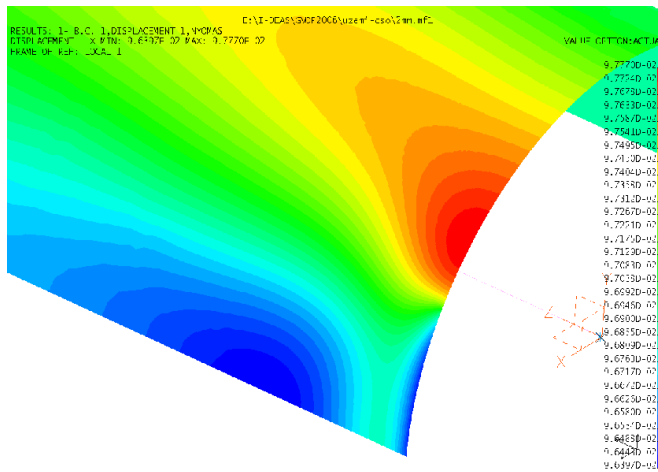
Figure 11. Radial displacements at internal failure with 2 mm depth

the radial displacements in the case of external failure for the three investigated failure depths. In this case the distribution of the deformations do not depend on the depth of external failure. Naturally, the magnitudes of deformation are different.   The different distributions of deformations for internal and external failure will play a very important role at the repair.

Table 4 summarizes the critical strain and von Mises reduced stress values for the hazardous experimental loading case at internal failure. Compering the $\varepsilon_{z\ max}$ axial and
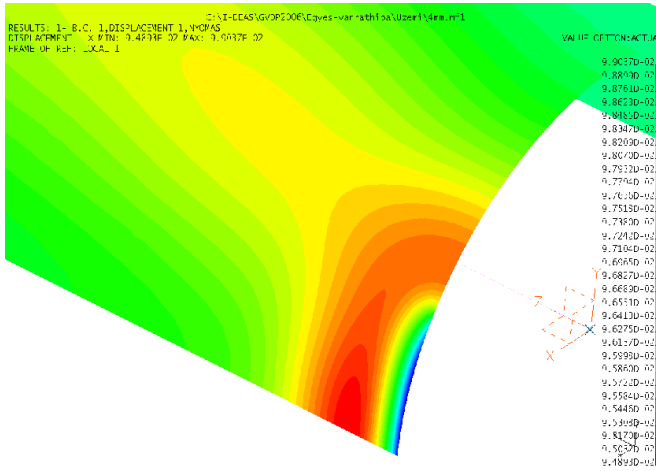
Figure 12. Radial displacements at internal failure with 4 mm depth
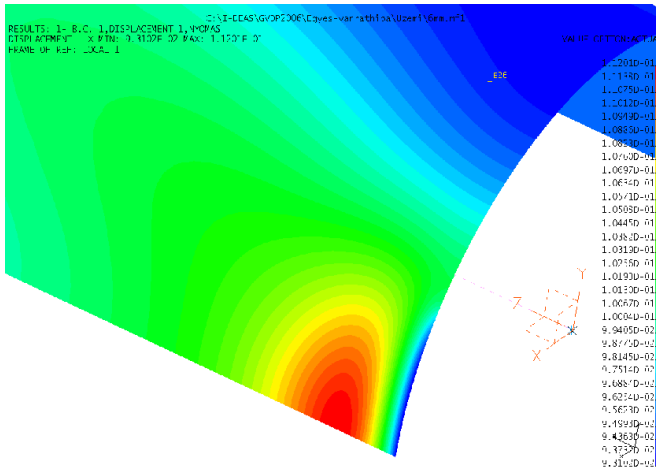
Figure 13. Radial displacements at internal failure with 6 mm depth

$\varepsilon_{\varphi\,max}$ circular strains it is seen that they are in the same order of magnitude at lower depths. However the $\varepsilon_{z\,max}$ axial strains become dominant at increasing failure depth. Therefore one can state that the influence of axial loading is dominant for strains around the circular failure at higher depths.
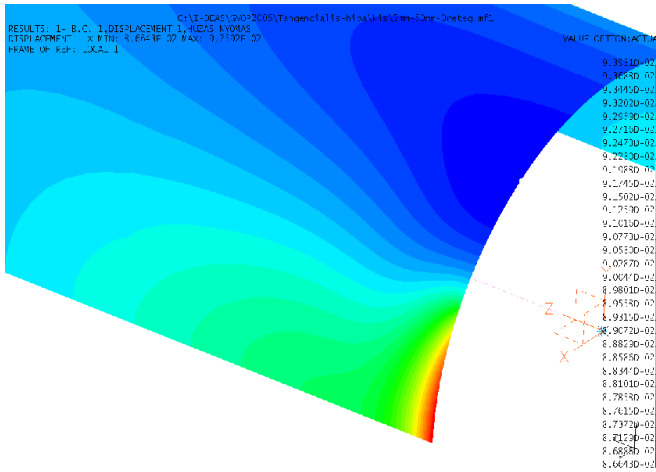
Figure 14. Radial displacements at external failure with 2 mm depth
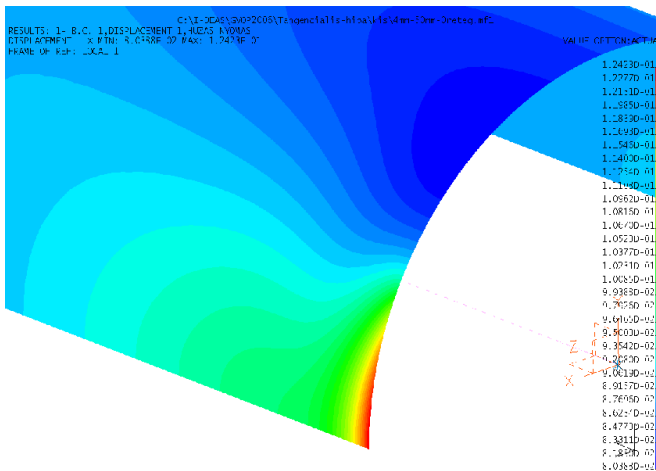
Figure 15. Radial displacements at external failure with 4 mm depth

The maximum reduced stresses computed by different models are close to each other below the yield stress, in cases of 2 and 4 mm deep internal failures. At 4 mm failure depth the maximum reduced stresses reach or are close to the yield stress value. For 6 mm failure depth every model, including the shell model, indicates the fracture of the pipe.
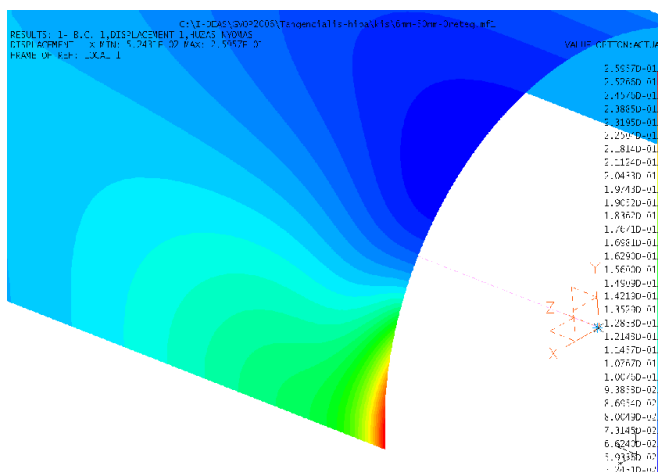
Figure 16. Radial displacements at external failure with 6 mm depth

Therefore the damaged pipe needs repair only at 6 mm failure depth. Table 5 summarizes

Depth [mm]	Quantity [Dimension]	Shell model	3D elastic model	3D elasto-plastic model
2	$\varepsilon_{\varphi\,max}$ [1]	$1{,}2603 \cdot 10^{-3}$	$9{,}3827 \cdot 10^{-4}$	$9{,}3827 \cdot 10^{-4}$
	$\varepsilon_{z\,max}$ [1]	$1{,}0610 \cdot 10^{-3}$	$1{,}2283 \cdot 10^{-3}$	$1{,}2283 \cdot 10^{-3}$
	$\sigma_{red\,max}$ [MPa]	222,37	243,03	243,03
4	$\varepsilon_{\varphi\,max}$ [1]	$2{,}4310 \cdot 10^{-3}$	$8{,}7135 \cdot 10^{-4}$	$8{,}7235 \cdot 10^{-4}$
	$\varepsilon_{z\,max}$ [1]	$7{,}2919 \cdot 10^{-3}$	$2{,}5820 \cdot 10^{-3}$	$2{,}5820 \cdot 10^{-3}$
	$\sigma_{red\,max}$ [MPa]	*502,38*	455,11	455,11
6	$\varepsilon_{\varphi\,max}$ [1]	$2{,}8736 \cdot 10^{-3}$	$9{,}3700 \cdot 10^{-4}$	$9{,}4239 \cdot 10^{-4}$
	$\varepsilon_{z\,max}$ [1]	$3{,}5439 \cdot 10^{-2}$	$6{,}7759 \cdot 10^{-3}$	$7{,}4800 \cdot 10^{-3}$
	$\sigma_{red\,max}$ [MPa]	**898,85**	**1191,4**	**603,0**

Table 4. Critical values - internal failures - experimental loading case

the characteristic critical strain and von Mises reduced stress values for the more hazardous experimental loading case at external failure. These results show very similar behavior from the point of view of strains and stresses for the external damaged pipe than for the internal failure. Also the external damaged pipe needs repair only at 6 mm failure depth. It is curious that though the deformations are different similar strain and stress values have been obtained for the internal and external failures.

Depth [mm]	Quantity [Dimension]	Shell model	3D elastic model	3D elasto-plastic model
2	$\varepsilon_{\varphi\,max}$ [1]	$8{,}9118 \cdot 10^{-4}$	$9{,}8610 \cdot 10^{-4}$	$9{,}8610 \cdot 10^{-4}$
	$\varepsilon_{z\,max}$ [1]	$7{,}2939 \cdot 10^{-4}$	$1{,}1496 \cdot 10^{-3}$	$1{,}1496 \cdot 10^{-3}$
	$\sigma_{red\,max}$ [MPa]	196,39	233,38	233,38
4	$\varepsilon_{\varphi\,max}$ [1]	$1{,}1614 \cdot 10^{-3}$	$1{,}1841 \cdot 10^{-3}$	$1{,}1841 \cdot 10^{-3}$
	$\varepsilon_{z\,max}$ [1]	$2{,}5196 \cdot 10^{-3}$	$2{,}7328 \cdot 10^{-3}$	$2{,}7328 \cdot 10^{-3}$
	$\sigma_{red\,max}$ [MPa]	*531,40*	490,62	490,62
6	$\varepsilon_{\varphi\,max}$ [1]	$1{,}4874 \cdot 10^{-3}$	$1{,}6668 \cdot 10^{-3}$	$1{,}6706 \cdot 10^{-3}$
	$\varepsilon_{z\,max}$ [1]	$4{,}8891 \cdot 10^{-3}$	$5{,}5436 \cdot 10^{-3}$	$7{,}1033 \cdot 10^{-3}$
	$\sigma_{red\,max}$ [MPa]	**1009,7**	**973,58**	**603,0**

Table 5. Critical values - external failures - experimental loading case

All the three applied models indicate the fracture of the pipe for the same failure depth. From here on the simplest multilayered shell model is used in the investigation of repaired cases because it needs less numerical efforts than the others.

5.3. Results of repaired pipes

As it is determined in 5.2 the axial loading becomes dominant at both increasing internal and external circular failure depths. This dominant loading results very different deformations at internal (Fig. 17.) and external (Fig. 18.) failure. The highest radial deformations occur shifted in axial direction nearby the internal failure and exactly in the middle of the external failure.

The phenomenon can be explained by Fig. 19. If there is no failure in the pipe wall the stress resultant over the thickness is only the N_a force. In the undamaged case there is no bending effect in the pipe wall.

However in the case of internal failure the stress resultants provide a N_a force and an additional M_{ti} bending moment. This bending moment opens the internal failure and results maximum radial deformations shifted nearby the failure. in the case of external failure the stress resultants provide a N_a force and an additional M_{to} bending moment. This bending moment also opens the external failure and results maximum radial deformations in the middle of the failure. Both internal and external failures can be fixed from the outside or from the inside. Fig. 20. shows the repair versions for an internal failure. The pipe can be considered as fixed if the $\sigma_{red\,max}$ reduced stresses in the steel wall do not reach the yield stress value (3.3) and the K_{tw} Tsai-Wu failure coefficient in the reinforcement do not reach the value 1 (3.7).
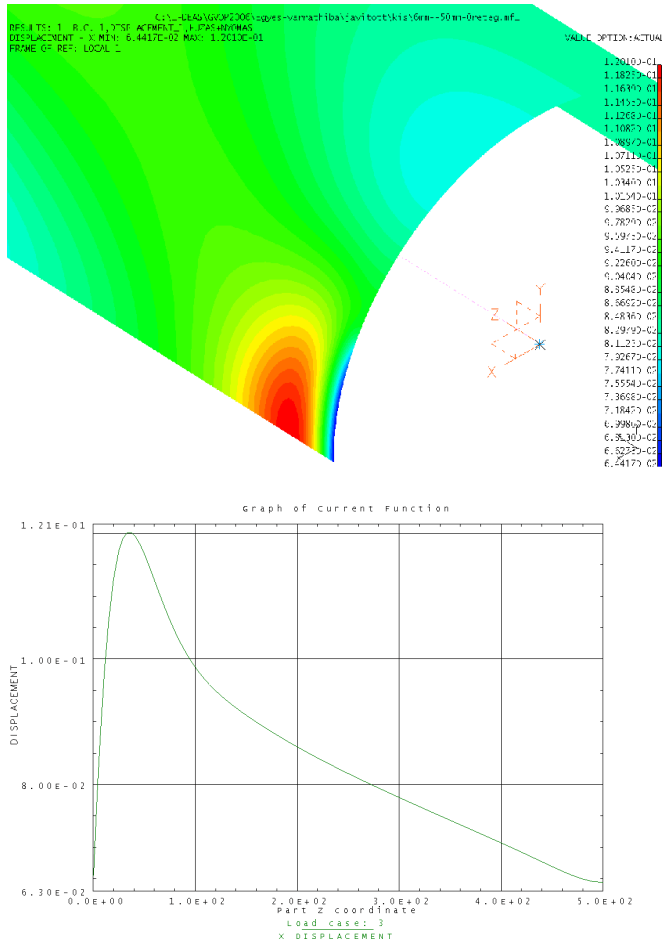
Figure 17. Radial displacements at internal failure with 6 mm depth

Computations are carried out for repaired internal failure by 50, 100 and 200 mm bandwidth of CFRP layers. The numerical results proved that the bandwidth in this range practically does not influence the behavior of repaired case.

Table 6. summarizes the numerical results for a 6 mm deep internal failure with 50 mm bandwidth reinforcement, in the left two columns for external reinforcement and in the right two columns for internal reinforcement. It can be seen from Table 6. that an internal
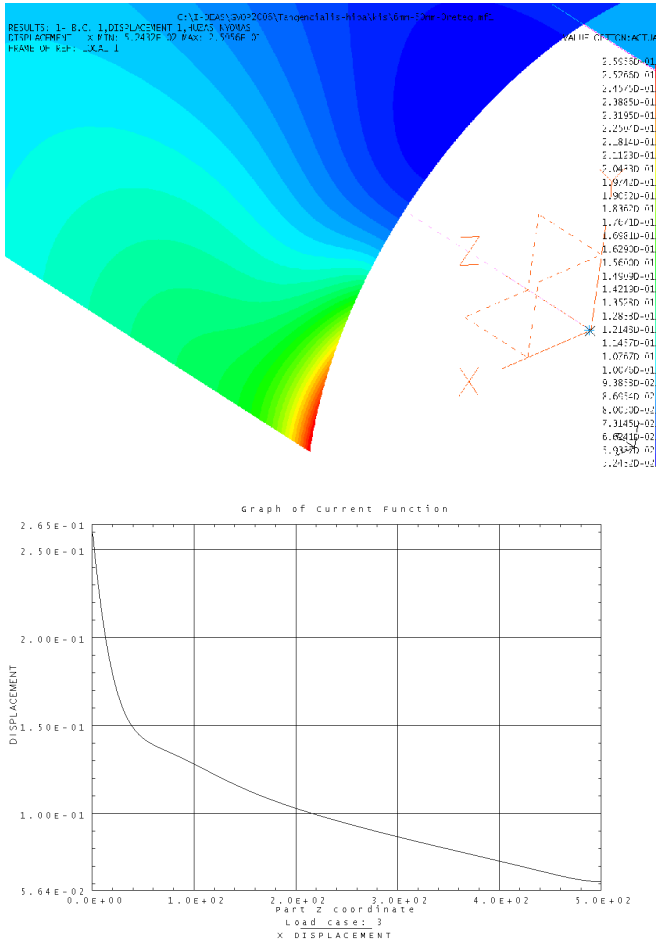
Figure 18. Radial displacements at external failure with 6 mm depth

circular failure can be repaired better by internal reinforcement than by external one. Both goals for failure criteria (3.3) and (3.87) can already be fulfilled by 8 layers of internal winding. The external reinforcement with a low number of layers makes the situation worse and the pipe can only be fixed with a very high number of layers.

This phenomenon can be explained by Fig. 20. With a lower number of external layers the e eccentricity is increased by the reinforcement which makes the M_{ti} local bending
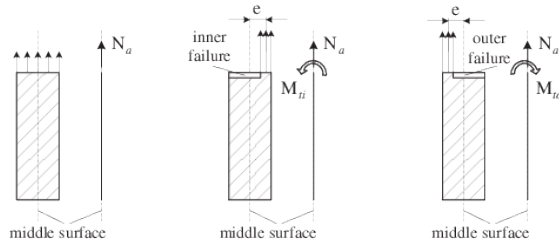
Figure 19. Force and moment resultants at internal and external failure
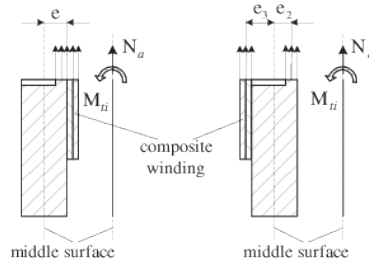
Figure 20. Repairing the internal failure by composite winding

moment higher but a high enough number of layers can compensate this action. However the internal reinforcement creates an opposite bending moment by e_3 eccentricity which can balance the original bending moment.

Table 7. summarizes the numerical results for a 6 mm deep external failure with 50 mm bandwidth reinforcement, in the left two columns for external reinforcement and in the right two columns for internal reinforcement. When repairing external circular failure the situation is the opposite to the previous case. It is seen from Table 7 that an external circular failure can be repaired better by external reinforcement than by internal one. Also in this case both failure criteria can already be fulfilled by 8 layers of external winding. The internal reinforcement with a low number of layers makes the situation worse and the pipe can be fixed only with a very high number of layers. The argument for this phenomenon is the same as given at internal failures.

6. Conclusions

The conclusions of the numerical investigation are the following:

Number of layers/ thickness [mm]	$\sigma_{\text{red max}}^{\text{external}}$ [MPa]	$K_{\text{tw}}^{\text{external}}$ [–]	$\sigma_{\text{red max}}^{\text{internal}}$ [MPa]	$K_{\text{tw}}^{\text{internal}}$ [–]
0/0	908	–	908	–
4/1,2	1046,0	0,6137	600,2	0,0641
8/2,4	984,4	0,7704	499,1	-0,0187
12/3,6	804,6	0,4633	–	–
16/4,8	674,1	0,2729	–	–
20/6,0	586,0	0,1909	–	–
24/7,2	523,0	0,1188	–	–
28/8,4	475,5	0,0862	–	–

Table 6. Reduced stresses and failure coefficients for internal failure with 6 mm depth

Number of layers/ thickness [mm]	$\sigma_{\text{red max}}^{\text{external}}$ [MPa]	$K_{\text{tw}}^{\text{external}}$ [–]	$\sigma_{\text{red max}}^{\text{internal}}$ [MPa]	$K_{\text{tw}}^{\text{internal}}$ [–]
0/0	1009,7	–	1009,7	–
4/1,2	550,2	0,0704	1125,5	0,7026
8/2,4	499,2	0,0111	1017,3	0,8056
12/3,6	–	–	825,1	0,4745
16/4,8	–	–	692,3	0,2791
20/6,0	–	–	602,8	0,1807
24/7,2	–	–	539,4	0,1280
28/8,4	–	–	491,9	0,0974

Table 7. Reduced stresses and failure coefficients for external failure with 6 mm depth

- From the engineering point of view the multilayered shell model is a suitable tool for numerical analysis of pipe failures and for investigation of repaired pipes.

- From the mechanical point of view the the insulation layer is negligible.

- The experimental loading case is more hazardous than the normal working conditions.

- The critical strains and stresses are similar at internal and external circular failures, however the character of deformations is different.

- It is sufficient to use only a few number of CFRP layers for repair of very deep circular failures, if they are applied from the failure side.

- The internal and external failures have to be fixed by internal and external reinforcement, respectively.

- The bandwidth in the investigated range of composite layers does not play an important role at the repair of circular failure.

Acknowledgment

References

[1] Reddy, J. N.: *Mechanics of laminated composite plates and shells, Theory and Analysis*, CRC Press (2004).

[2] Matthews, F. L., Davies, G. A. O., Hitchings, D., Soutis, C.: *Finite element modelling of composite materials and structures*, Woodhead Publishing Ltd, Camgridge (2000).

[3] Bathe, K. J.: *Finite Element Procedures*, Prentice Hall International Editions (1996).

[4] *I-DEAS User' Guide*, UGS PLM Solutions Inc. (2004).

[5] Égert, J., Pere, B., Molnár-Égert, É.: *Csövek varrathibái textil kompozitos javításának szilárdságtani vonatkozásai (Mechanical aspects of reinforcements of pipeline welding failures by fabrics)*. EMT Műszaki Szemle (EMT Technical Rewiev), (2008), pp 125–131. (in Hungarian)

[6] Pere, B., Égert, J.: *Finite Element modelling opportunities of artificial welding failures and external damage of pipelines*. Proc. microCAD 2008 Int. Sci. Conf. 20-21 March 2008., Section F: Applied Mechanics, pp 39–44.

[7] Lukács, J., Nagy, Gy. and Török, I.: *Kísérleti csőszakaszok vizsgálata (Investigation of test pipe parts)* Polimer mátrixú kompozittal erősített hibrid csövek integritása - konferencia kiadvány (Integrity of hybride pipes reinforced by polymere matrix composite - Conf. Proc.) Miskolc-Egyetemváros, (2008), pp 174–193. (in Hungarian)

[8] Czél, G.: *Polimer kompozit csőanyagok sajátos anyagvizsgálati módszerei (Special material test methods for polymere composite pipe materials)* Polimer mátrixú kompozittal erősített hibrid csövek integritása - konferencia kiadvány (Integrity of hybride pipes reinforced by polymere matrix composite - Conf. Proc.) Miskolc-Egyetemváros, (2008), pp 17–24. (in Hungarian)